Cell Reports

Article

Molecular basis of glycyl-tRNA^{Gly} acetylation by TacT from *Salmonella* Typhimurium

Graphical abstract

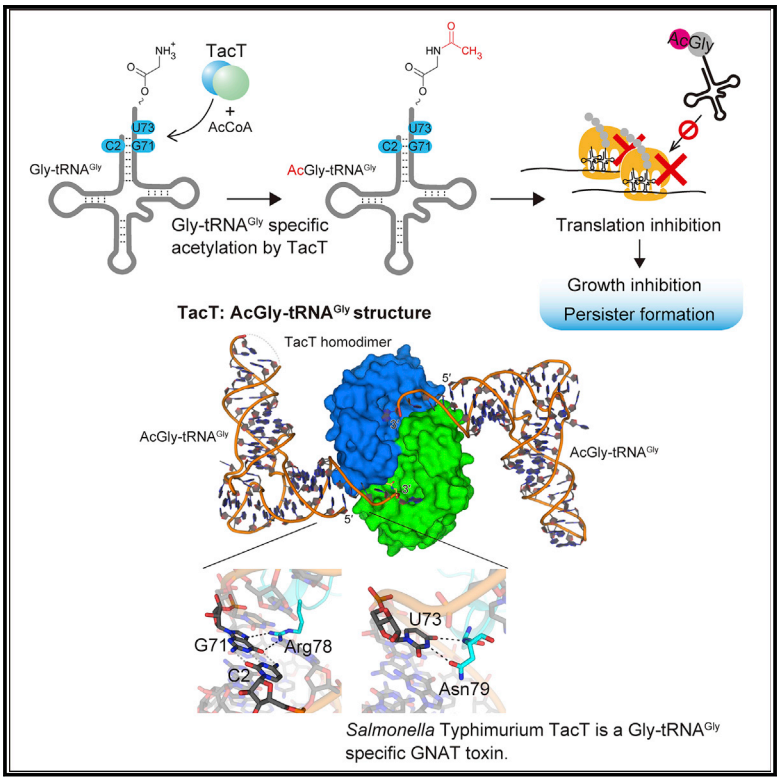

Highlights

- *Salmonella* TacT promotes persister formation through acetylation of aa-tRNA
- TacT exclusively acetylates Gly-tRNA^{Gly} *in vivo* and *in vitro*
- The crystal structure of TacT:acetyl Gly-tRNA^{Gly} complex is determined
- TacT recognizes U73 and G71 specific in tRNA^{Gly} and 3′-amino acid moiety

Authors

Yuka Yashiro, Chuqiao Zhang, Yuriko Sakaguchi, Tsutomu Suzuki, Kozo Tomita

Correspondence

kozo-tomita@edu.k.u-tokyo.ac.jp

In brief

Salmonella TacT toxin promotes persister formation through acetylation of aminoacyl-tRNA in macrophages. Yashiro et al. show through structural and biochemical analyses that TacT is a glycyl-tRNA^{Gly}-specific acetyltransferase, and it recognizes the specific sequence only found in tRNA^{Gly} and 3′-amino acid moiety and discriminates from other aminoacyl-tRNAs.

Yashiro et al., 2021, Cell Reports *37*, 110130
December 21, 2021
https://doi.org/10.1016/j.celrep.2021.110130

CellPress

Cell Reports

CellPress
OPEN ACCESS

Article

Molecular basis of glycyl-tRNA^{Gly} acetylation by TacT from *Salmonella* Typhimurium

Yuka Yashiro,[1] Chuqiao Zhang,[1] Yuriko Sakaguchi,[2] Tsutomu Suzuki,[2] and Kozo Tomita[1,3,*]

[1]Department of Computational Biology and Medical Sciences, Graduate School of Frontier Sciences, The University of Tokyo, Kashiwa, Chiba 277-8562, Japan

[2]Department of Chemistry and Biotechnology, Graduate School of Engineering, The University of Tokyo, Bunkyo-ku, Tokyo 113-8656, Japan

[3]Lead contact

*Correspondence: kozo-tomita@edu.k.u-tokyo.ac.jp

https://doi.org/10.1016/j.celrep.2021.110130

SUMMARY

Bacterial toxin-antitoxin modules contribute to the stress adaptation, persistence, and dormancy of bacteria for survival under environmental stresses and are involved in bacterial pathogenesis. In *Salmonella* Typhimurium, the Gcn5-related *N*-acetyltransferase toxin TacT reportedly acetylates the α-amino groups of the aminoacyl moieties of several aminoacyl-tRNAs, inhibits protein synthesis, and promotes persister formation during the infection of macrophages. Here, we show that TacT exclusively acetylates Gly-tRNA^{Gly} *in vivo* and *in vitro*. The crystal structure of the TacT:acetyl-Gly-tRNA^{Gly} complex and the biochemical analysis reveal that TacT specifically recognizes the discriminator U73 and G71 in tRNA^{Gly}, a combination that is only found in tRNA^{Gly} isoacceptors, and discriminates tRNA^{Gly} from other tRNA species. Thus, TacT is a Gly-tRNA^{Gly}-specific acetyltransferase toxin. The molecular basis of the specific aminoacyl-tRNA acetylation by TacT provides advanced information for the design of drugs targeting *Salmonella*.

INTRODUCTION

Bacterial toxin-antitoxin (TA) modules are operons consisting of toxin and antitoxin gene pairs and are widely present in bacteria (Goeders and Van Melderen, 2014; Harms et al., 2016, 2018; Page and Peti, 2016; Pandey and Gerdes, 2005). According to the nature of the antitoxin and the mechanism by which it neutralizes the toxin activity, TA modules are classified into six types (type-I–VI) (Hayes and Van Melderen, 2011; Yamaguchi and Inouye, 2011). In type-II TA modules, under normal physiological conditions, the proteinous toxin function is neutralized by the proteinous cognate antitoxin through protein-protein interactions, thus suppressing the toxin activity. Upon environmental stresses, such as nutrient starvation, DNA damage, and antibiotic exposure, the proteolytically susceptible antitoxins are degraded and the suppression of toxin activity by the antitoxin is released, leading to the toxin activation (Hayes and Van Melderen, 2011; Muthuramalingam et al., 2016).

Toxins in TA modules cause bacterial cell growth arrest by targeting essential cellular processes, including DNA replication, transcription, translation, and cell wall synthesis (Harms et al., 2016). TA modules in bacteria contribute to their survival under various conditions, by suppressing their growth upon stresses and inducing their dormancy (Gerdes et al., 1986; Harms et al., 2016; Maisonneuve and Gerdes, 2014; Yamaguchi and Inouye, 2011). TA modules are considered to participate in antibiotic persistence (Cheverton et al., 2016; Helaine et al., 2014; Helaine and Kugelberg, 2014; Maisonneuve and Gerdes, 2014; Rycroft et al., 2018), a phenomenon in which a small fraction of antibiotic-exposed bacteria exhibits multidrug tolerance without any genetic alterations (Balaban et al., 2004; Helaine and Kugelberg, 2014; Mulcahy et al., 2010). Antibiotic persistence causes the recalcitrance and relapse of bacterial infections after antibiotic treatment. Thus, understanding the mechanism of action of the toxin in the TA modules of pathogenetic bacteria is particularly important from pathological and clinical aspects.

During the past several years, a new type-II TA module in which the toxin belongs to the Gcn5-related *N*-acetyltransferase (GNAT) family was identified in various bacteria (Cheverton et al., 2016; Jurėnas et al., 2017a, 2017b; McVicker and Tang, 2016; Ovchinnikov et al., 2020; Qian et al., 2018; Rycroft et al., 2018; Wilcox et al., 2018; Yeo, 2018). The GNAT toxin family includes AtaT and AtaT2 from enterohemorrhagic *Escherichia coli* O157:H7 (Jurėnas et al., 2017a; Ovchinnikov et al., 2020); ItaT from the *E. coli* HS strain (Wilcox et al., 2018); TacT, TacT2, and TacT3 from *Salmonella* Typhimurium and *Salmonella* Enteritidis (Cheverton et al., 2016; Rycroft et al., 2018); KacT from *Klebsiella pneumoniae* (Qian et al., 2018; Yeo, 2018); GmvT from *Shigella sonnei* (McVicker and Tang, 2016), and others. GNAT toxins acetylate the α-amino group of the aminoacyl moiety of aminoacyl-tRNAs (aa-tRNAs), using acetyl-coenzyme A (AcCoA) as the acetyl group donor, thus inhibiting cellular protein synthesis. The GNAT toxins from various bacteria reportedly target different aminoacyl-tRNA species and diverge in their specificities toward aminoacyl-tRNAs (Jurėnas et al., 2017a; Ovchinnikov et al., 2020; Rycroft et al., 2018; Yashiro et al., 2020; Zhang et al., 2020). However, the molecular basis for the different substrate specificities of the GNAT family toxins has remained elusive.

ItaT from the *E. coli* HS strain reportedly acetylates several aminoacyl-tRNAs charged with hydrophobic amino acids, such as Ile-tRNA^{Ile} and Val-tRNA^{Val}, in addition to Met-tRNA^{Met} *in vitro* and *in vivo*, and the size and shape of the hydrophobic pocket for the accommodation of the aminoacyl moieties of aminoacyl-tRNAs would presumably specify the substrate for acetylation by ItaT (Zhang et al., 2020). The genome of enterohemorrhagic *E. coli* O157:H7 strain has two GNAT class TA modules, *ataRT* and *ataR2T2*. AtaT toxin acetylates several aminoacyl-tRNAs charged with hydrophobic and bulky amino acids, such as Trp-tRNA^{Trp}, Phe-tRNA^{Phe}, and Tyr-tRNA^{Tyr}, in addition to Gly-tRNA^{Gly}, *in vivo* and *in vitro*. Very recently the structure of AtaT complexed with the acetylated methionyl-tRNAf^{Met} was determined, and together with the biochemical analyses, it was shown that AtaT specifically recognizes the consecutive G-C pairs in the bottom half of the acceptor stem of aminoacyl-tRNAs. AtaT also recognizes the properties of the aminoacyl moieties of aminoacyl-tRNAs. Thus, the substrate selection by AtaT was suggested to be governed by the specific acceptor stem sequence of tRNA and the properties of the aminoacyl moieties of aminoacyl-tRNAs (Yashiro et al., 2020). On the other hand, AtaT2 was suggested to acetylate Gly-tRNA^{Gly} specifically *in vivo*, through a ribosome-profile analysis in AtaT2-induced cells; however, the mechanism of the specific acetylation of Gly-tRNA^{Gly} by AtaT2 has remained elusive (Ovchinnikov et al., 2020).

The genomes of *Salmonella* Typhimurium and *Salmonella* Enteritidis contain three GNAT toxin genes: TacT, TacT2, and TacT3 (Cheverton et al., 2016; Rycroft et al., 2018). The deletion of each GNAT TA module in *Salmonella* was shown to reduce persister formation upon internalization by macrophage (Cheverton et al., 2016; Helaine et al., 2014; Rycroft et al., 2018). Thus, the GNAT toxins in *Salmonella* species are involved in persister formation during the infection of macrophages (Cheverton et al., 2016; Helaine et al., 2014; Rycroft et al., 2018), which could cause a relapse of the infection after antibiotic treatment. *In vitro*, TacT, TacT2, and TacT3 acetylated several kinds of isoaccepting aminoacyl-tRNAs and inhibited the elongation process of protein synthesis (Cheverton et al., 2016; Rycroft et al., 2018). These toxins reportedly acetylated overlapping aminoacyl-tRNA species, but with different efficiencies. However, the molecular mechanisms of the preference and selectivity toward aminoacyl-tRNAs by these toxins have remained elusive.

We now present the molecular basis of aminoacyl-tRNA recognition by *Salmonella* Typhimurium TacT. In contrast to the previous report (Rycroft et al., 2018), we show that TacT exclusively acetylates Gly-tRNA^{Gly} isoacceptors *in vivo* and *in vitro*. Our structural analyses of TacT complexed with acetyl-Gly-tRNA^{Gly} and biochemical analyses reveal the molecular basis for the specific acetylation of Gly-tRNA^{Gly} by TacT. The detailed mechanism of the specific Gly-tRNA^{Gly} acetylation provides crucial information for the development of drugs that restart the growth of the persister cells and restore their antibiotic susceptibility.

RESULTS

TacT selectively acetylates Gly-tRNA^{Gly} isoacceptors

To analyze the substrate aminoacyl-tRNAs of TacT in the context of the cellular environment, we utilized *E. coli* strain MG1655. The *E. coli* MG1655 chromosome is devoid of the GNAT toxin gene, whereas *Salmonella* Typhimurium chromosome has three GNAT toxin genes: TacT, TacT2, and TacT3. Since *E. coli* and *Salmonella* share similar genomic tRNA sequences (Chan and Lowe, 2016; Jühling et al., 2009) (Figure S1), we utilized the *E. coli* MG1655 strain to analyze the aminoacyl-tRNA substrates acetylated by the ectopically expressed TacT protein *in vivo*. TacT was expressed in *E. coli* MG1655 by the pBAD plasmid system, in which TacT expression is inducible by arabinose. To analyze the intracellular aminoacyl-tRNAs acetylated by the action of TacT, the RNA fractions were extracted from the cells with or without TacT induction, under acidic conditions. The fractions were then treated with stable isotopic acetic anhydride-D6 ($(CD_3CO)_2O$, where D is deuterium) to chemically acetylate the remaining aminoacyl-tRNAs that were not acetylated by the action of TacT in cells. The RNAs were then digested with RNase I, and the hydrolysates were analyzed by liquid chromatography-mass spectrometry (LC-MS) (Yashiro et al., 2020; Zhang et al., 2020) (Figure 1A).

The LC-MS analysis showed that the molecular mass corresponding to acetyl-Gly-A76 (Ac-Gly-A76; *m/z* 367.13, z = +1) was detected in the RNase-I-digested RNAs from cells with TacT induction. In the control cells without TacT induction, the molecular mass corresponding to Ac-Gly-A76 was not detected, but that corresponding to D3AcGly-A76 (*m/z* 370.15, z = +1) was observed (Figure 1B). Thus, Gly-tRNA^{Gly} isoacceptors are acetylated by the action of TacT *in vivo*. The fractions of each aminoacyl-tRNA acetylated by the action of TacT were estimated by quantifying the ratio of the peak areas corresponding to acetyl-aminoacyl-A76 (Ac-aa-A76) and D3Ac-aa-A76 for each aminoacyl-tRNA (Figure 1C). The results showed that more than 80% of Gly-tRNA^{Gly} was acetylated at 10 min after the induction of TacT, but none of the other aminoacyl-tRNAs were acetylated even at 60 min after the induction (Figure 1C). These results suggest that TacT mainly targets Gly-tRNA^{Gly} isoacceptors *in vivo*.

In a previous *in vitro* study, besides the acetylation of Gly-tRNA^{Gly} isoacceptors, TacT also acetylated isoaccepting tRNAs for Ile/Leu, Trp, and Ser, when the TacT protein was added to an *E. coli* cell-free translation system (Rycroft et al., 2018). To further verify the substrate preference of TacT, we examined the *in vitro* acetylation of several kinds of aminoacyl-tRNA species from *E. coli* and compared the initial velocities of the acetylation of each aminoacyl-tRNA. The steady-state kinetics of Gly-tRNA^{Gly} acetylation by TacT showed that the K_M value of Gly-tRNA^{Gly} was approximately 50.9 μM (Figure S2). The concentration of each aminoacyl-tRNA (10 μM) used for the assay is lower than the K_M value of Gly-tRNA^{Gly}. Thus, the conditions would have sufficient sensitivity to evaluate the substrate preference of TacT. The results showed that TacT acetylated Gly-tRNA^{Gly} isoacceptors efficiently, in contrast to the isoacceptors of Ala-tRNA^{Ala}, Cys-tRNA^{Cys}, Ile-tRNA^{Ile}, Leu-tRNA^{Leu}, Trp-tRNA^{Trp}, Ser-tRNA^{Ser}, Gln-tRNA^{Gln}, and Phe-tRNA^{Phe} (Figures 1D and 1E). A slight amount of Cys-tRNA^{Cys} acetylation was detected in the time course of the reaction, but the rate of Cys-tRNA^{Cys} acetylation was ~2% of that of Gly-tRNA^{Gly} (Figure 1E). The acetylation of the other tested aminoacyl-tRNAs was almost undetectable.

These results demonstrated that TacT is highly selective toward Gly-tRNA^{Gly} isoacceptors *in vivo* and *in vitro*. In *Salmonella*

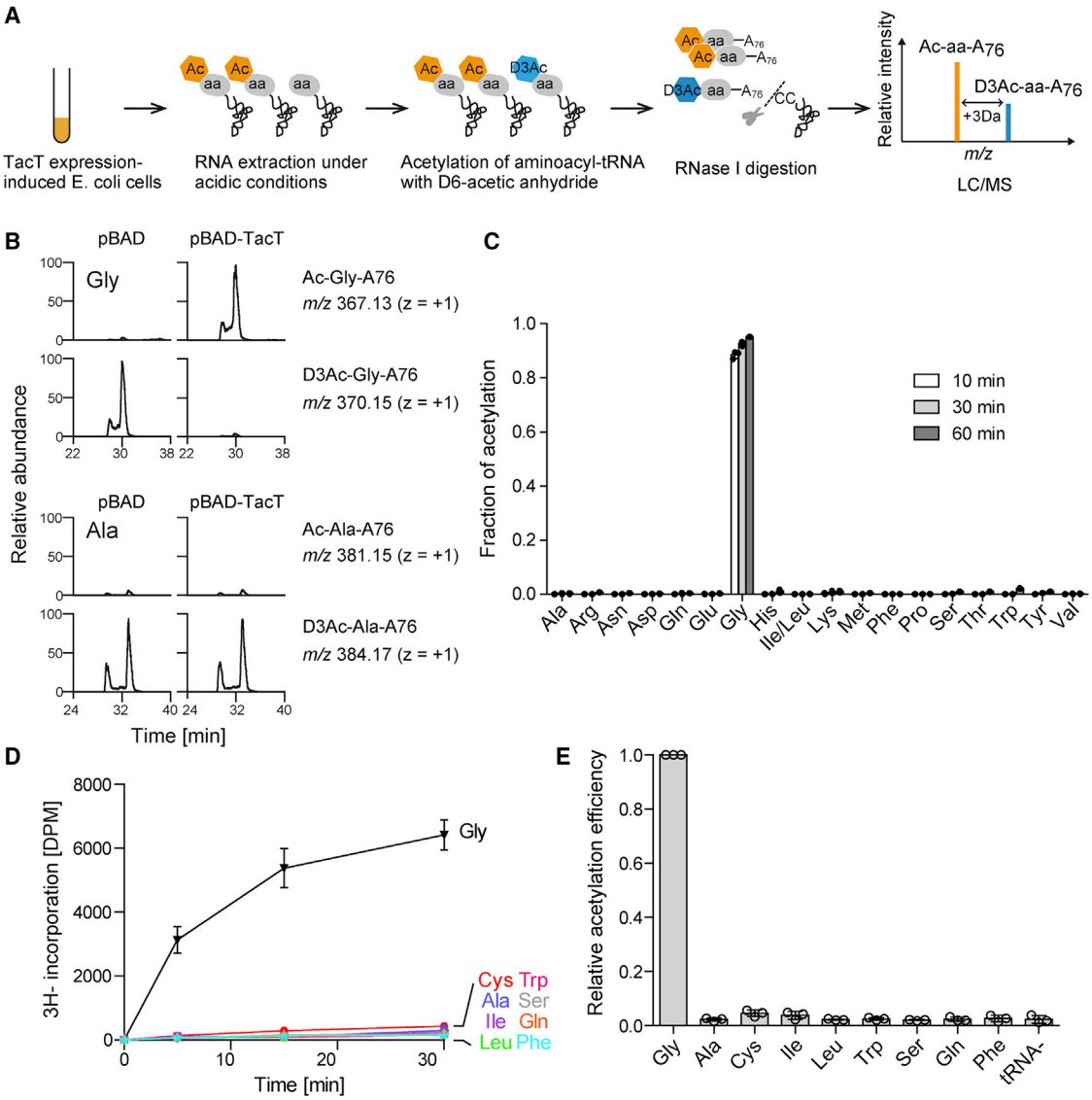

Figure 1. Acetylation of glycyl-tRNA^{Gly} by TacT

(A) Schematic diagram of the LC-MS detection and quantification of aminoacyl-tRNAs acetylated by TacT (Yashiro et al., 2020).

(B) LC-MS analysis of RNase-I-digested fragments of acetyl-aminoacyl-tRNAs after 30 min of induced TacT expression (pBAD-TacT) and the negative control (pBAD). Extracted ion chromatograms of the proton adducts corresponding to Ac-Gly-A76 (*m/z* = 367.13), D3Ac-Gly-A76 (*m/z* = 370.15), Ac-Ala-A76 (*m/z* = 381.15), and D3Ac-Ala-A76 (*m/z* = 384.17), derived from AcGly-tRNA^{Gly}, D3AcGly-tRNA^{Gly}, AcAla-tRNA^{Ala}, and D3AcAla-tRNA^{Ala}, respectively. The two peaks observed for each Ac-aa-A76 are likely attributable to structural isomers of 3′-acetyl-aminoacyl-A76 and 2′-acetyl-aminoacyl-A76 (Yang et al., 2006).

(C) Fractions of aminoacyl-tRNAs acetylated by TacT *in vivo*. The amounts of Ac-aa-A76 and D3Ac-aa-A76, after 10, 30, and 60 min of TacT expression induction, were quantified, and the fractions of individual aminoacyl-tRNAs acetylated by TacT *in vivo* were estimated as the ratio of Ac-aa-A76 to the sum of the amounts of Ac-aa-A76 and D3Ac-aa-A76. The bars in the graph are SD of three independent (n = 3) experiments, and the data are presented as mean values ± SD.

(D) Time courses of the acetylation of various aminoacyl-tRNAs by TacT. The bars in the graphs are SD of three independent (n = 3) experiments.

(E) Relative acetylation rates of aminoacyl-tRNAs (10 μM) tested in (D) by TacT. The reactions were incubated for 5 min at 37°C, and the acetylation efficiency of the Gly-tRNA^{Gly} isoacceptor was taken as 1.0. The bars in the graph are SD of three independent (n = 3) experiments, and the data are presented as mean values ± SD.

cells, TacT would also target Gly-tRNA^{Gly} specifically, because TacT discriminates Gly-tRNA^{Gly} by recognizing specific sequences in tRNA^{Gly} as described below, and the sequences of tRNA^{Gly} isoacceptors are conserved between *E. coli* and *Salmonella* (Figure S1).

Structure determination of TacT complexed with AcGly-tRNA^{Gly}

To elucidate the molecular mechanism of the selective acetylation of Gly-tRNA^{Gly} by TacT, we co-crystallized the catalytic mutant TacT with the Y140F mutation (Cheverton et al., 2016),

Table 1. Summary of data collection and refinement statistics

Data collection	
Space group	$P2_1$
Cell dimensions	
a, b, c (Å)	52.743, 121.873, 127.257
α, β, γ (°)	90, 91.069, 90
Wavelength (Å)	1.0000
Resolution (Å)[a]	49.05–3.10 (3.21–3.10)
R_{sym}[a]	0.237 (1.411)
I/σI[a]	7.6 (1.3)
$CC_{1/2}$[a]	0.994 (0.606)
Completeness (%)[a]	99.3 (98.0)
Redundancy[a]	7.1 (7.3)
Refinement	
Resolution (Å)	48.4–3.098 (3.209–3.098)
No. of reflections	29,068 (2821)
R_{work}/R_{free} (%)	20.85/26.34
No. of atoms	11,302
Protein	4,914
tRNA	6,347
Calcium ion	41
B-factors (Å^2)	
Protein	55.841
tRNA	85.777
Calcium ion	86.568
RMSDs	
Bond lengths (Å)	0.006
Bond angles (°)	1.05

R_{sym}=∑(hkl)∑i|I_i (hkl)-<I(hkl)>|/∑(hkl)∑i<I_i (hkl)>; I/σI= <I(hkl)>/[(1/N)∑ iσ_i (hkl)^2]^(1/2); R_{work}=∑(hkl)||Fobs(hkl)|-|Fcalc(hkl)||/∑(hkl)|Fobs(hkl)|; R_{free}= as for R_{work}, calculated for 5.0% of the total reflections.; $CC_{1/2}$, the Pearson's correlation coefficient calculated between two random half data sets; RMSD, root-mean-square deviation.
[a]Values in parentheses are for the highest-resolution shell.

TacT (Y140F), with acetylated Gly-tRNA^{Gly} (AcGly-tRNA^{Gly}) and determined the structure. AcGly-tRNA^{Gly} was used instead of Gly-tRNA^{Gly}, as the *N*-acetylation of an aminoacyl-tRNA stabilizes the ester bond between the amino acid and the tRNA (Walker and Fredrick, 2008). We successfully obtained the crystals of TacT (Y140F) complexed with AcGly-tRNA^{Gly}. The crystal belongs to the space group *P21* and contains two TacT dimers and four AcGly-tRNA^{Gly} molecules in the asymmetric unit (Figure S3A). The initial phases were determined by the molecular replacement method, using the TacT homodimer structure (Cheverton et al., 2016) (PDB: 5FVJ) (https://doi.org/10.2210/pdb5fvj/pdb) and a tRNA^{Gly} model generated from the structure of *E. coli* tRNA^{Phe} (PDB: 3L0U) (https://doi.org/10.2210/pdb3l0u/pdb) as search models. The structure was model built and finally refined to an *R* factor of 20.9% (R_{free} = 26.3%) at 3.1 Å resolution. Detailed statistics of the crystallographic data collection and refinement are provided in Table 1.

Overall structure of TacT complexed with AcGly-tRNA^{Gly}

In the structure of the TacT(Y140F):AcGly-tRNA^{Gly} complex, two tRNA^{Gly} molecules (tRNA$_a$ and tRNA$_b$) associate with one TacT homodimer (TacT$_a$ and TacT$_b$) (Figure 2A). Each tRNA^{Gly} molecule interacts with the positively charged surface area spanning the dimer interfaces of the TacT homodimer (Figure 2B), as observed in the structure of the AtaT:AcMet-tRNAf^{Met} complex (Yashiro et al., 2019, 2020). The 3′-terminal single-stranded region and the top half of the acceptor stem, particularly the 3′ part of the stem in tRNA^{Gly}, interact with the continuous positively charged area between two TacT molecules (Figure 2B). Other regions of the tRNA molecule do not interact with TacT at all. The structure suggests that the dimeric form of TacT would be required for tRNA binding, as observed in other GNAT toxins such as AtaT and ItaT from *E. coli* (Yashiro et al., 2019, 2020; Zhang et al., 2020).

In the present structure, the electron density of the 3′-acetylglycine (AcGly) moiety of AcGly-tRNA^{Gly} was visible in only one tRNA^{Gly} molecule (tRNA$_a$) in the asymmetric unit (Figures S3B and S3C), and the AcGly moiety could be modeled in tRNA$_a$. The 3′-AcGly-A76 of tRNA^{Gly} is directed toward the opposite side of the catalytic site of TacT, as described below. Thus, the present structure would represent the post-reaction stage, in which the acetyl-group has been transferred from AcCoA to Gly-tRNA^{Gly}. At this stage, the byproduct CoA has been released from the TacT, and AcGly-A76 of AcGly-tRNA^{Gly} has flipped out from the catalytic pocket, but the tRNA body is still bound to TacT. Hereafter, we focus on one of the two tRNA^{Gly}s (tRNA$_a$) in which the 3′-AcGly-A76 was model built and describe the interactions between tRNA$_a$ and TacT dimer (TacT$_a$ and TacT$_b$).

Specific recognition of AcGly-tRNA^{Gly} by TacT

In the structure of the TacT:AcGly-tRNA^{Gly} complex, α1 in one subunit (TacT$_a$) and the loop containing α2 in another subunit (TacT$_b$) together interact with the 3′ single-stranded region and the top half of the acceptor of tRNA^{Gly} (Figure 2A). As described above, the 3′-AcGly-A76 part of AcGly-tRNA^{Gly} is not in the active pocket. The Nη atom of Arg91 in β3 and the Nζ atom of Lys33 in α1 of TacT$_a$ form hydrogen bonds with the phosphate groups of A76 and C75, respectively (Figure 2C). The 4-NH$_2$ group, the N3 atom, and the O2 atom of the C75 base form hydrogen bonds with the Oδ atom, the Nδ atom of Asn37, and the Nε atom of Trp29 in α1 of TacT$_a$, respectively. The 4-NH$_2$ group of the C75 base also forms a hydrogen bond with the main-chain carbonyl oxygen of Asn79 in another subunit, TacT$_b$ (Figure 2C). The C75 base is stacked with the side chain of Lys33 in α1 of TacT$_a$ and the main chain of Pro81 in the loop containing α2 in TacT$_b$. The 4-NH$_2$ group and the N3 atom of the C74 base form hydrogen bonds with the main-chain carbonyl oxygen of Arg77 and the main-chain amide of Met80 in the loop containing α2 of TacT$_b$ (Figure 2C). Thus, the 3′-C74C75A76 are specifically recognized by TacT through hydrogen bonds. The N3 and O4 atoms of the discriminator base U73 form hydrogen bonds with the Oδ atom and the main-chain amide of Asn79 in TacT$_b$, respectively (Figure 2D). The 5′ phosphate of tRNA^{Gly} hydrogen bonds with the Nζ atom of Lys36 in α1 of TacT$_a$. The O6 and N7 atoms of G1 form hydrogen bonds with the Nδ atom of Asn79 (Figure 2D), and the O6 atom also hydrogen bonds with

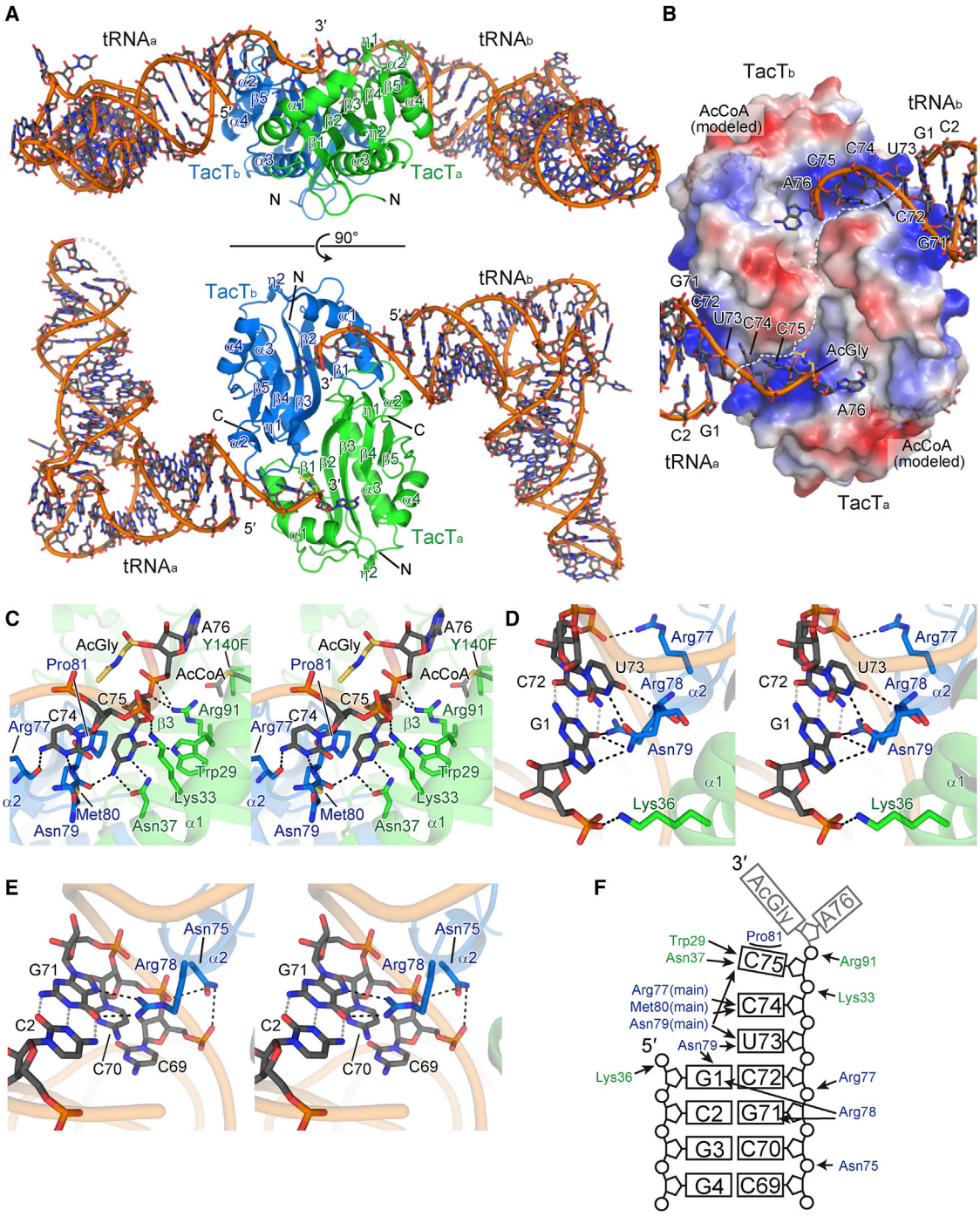

Figure 2. Structure of TacT complexed with AcGly-tRNA^{Gly}

(A) Overall structure of TacT complexed with acetyl-Gly-tRNA^{Gly} (AcGly-tRNA^{Gly}). TacT$_a$ (green) and TacT$_b$ (cyan) are shown in ribbon models, and AcGly-tRNA^{Gly} molecules (tRNA$_a$ and tRNA$_b$) are represented by stick models.

(B) Electrostatic surface area potentials of the TacT dimer in the complex with AcGly-tRNA^{Gly}. Positively and negatively charged areas are colored blue and red, respectively. Acetyl-CoA (AcCoA) molecules were modeled in the active sites of TacT dimer. AcGly-tRNA^{Gly}s are represented by stick models.

(C–E) Stereoviews of detailed interactions between TacT and AcGly-tRNA^{Gly}. TacT$_a$ and TacT$_b$ are colored as in (A). tRNA^{Gly} is shown as a stick model.

(F) Schematic representation of the interactions between TacT and AcGly-tRNA^{Gly}. Residues in TacT$_a$ and TacT$_b$ are colored green and cyan, respectively, as in (A).

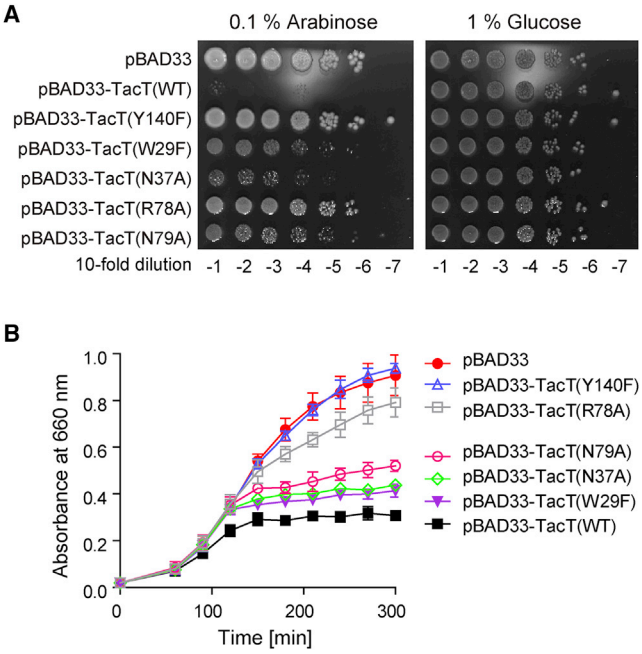

Figure 3. Toxicity of TacT variants in *E. coli*

(A) Overnight cultures of *E. coli* MG1655 transformed with pBAD33-TacT, and its variants were serially diluted. The dilutions were spotted on Luria broth (LB) agar plates containing 30 μg/mL chloramphenicol and supplemented with 0.1% (w/v) arabinose (left) or with 1% (w/v) glucose (right). The plates were incubated at 37°C overnight.

(B) Growth curves of *E. coli* MG1655 transformed with pBAD33-TacT and its variants. *E. coli* MG1655 transformed by pBAD33-TacT or its variants was inoculated in LB containing 30 μg/mL chloramphenicol and 0.1% (w/v) arabinose and incubated at 37°C. Bars in the graphs indicate the SD of three independent (n = 3) experiments.

the Nη atom of Arg78 in $TacT_b$. The phosphates of C70 and C72 form hydrogen bonds with the Nδ atom of Asn75 and the Nη atom of Arg77, respectively (Figures 2D and 2E). Arg78 in the loop containing α2 of $TacT_b$ protrudes into the minor groove of the acceptor helix. The Nη1 and Nη2 atoms of Arg78 form hydrogen bonds with the O6 and N7 atoms of G71, respectively (Figure 2E). Collectively, TacT recognizes the specific sequence in the top half of the acceptor of $tRNA^{Gly}$ through extensive hydrogen bonds (Figure 2F). In particular, as described below, the distinct recognition of the discriminator U73 and G71 in $tRNA^{Gly}$ by TacT is especially important for the specific acetylation of Gly-$tRNA^{Gly}$.

The glutamate mutants of some of the basic residues (Lys33, Lys36, Arg91, Arg77, and Arg78) of TacT, involved in the interaction with $tRNA^{Gly}$ in the present structure of the TacT:AcGly-$tRNA^{Gly}$ complex, reportedly attenuated the TacT toxicity when expressed in *Salmonella* cells (Cheverton et al., 2016). We further evaluated the involvement of several residues that form base-specific interactions with $tRNA^{Gly}$ in the present structure, in the toxicity of TacT in *E. coli*. The mutation of Arg78, which recognizes G71 of $tRNA^{Gly}$, to Ala (R78A) reduced the TacT toxicity to a similar extent as the Y140F catalytic mutant. The mutation of Asn79, which interacts with U73 of $tRNA^{Gly}$, to Ala (N79A) also decreased the TacT toxicity. In addition, the W29F and N37A TacT mutants also attenuated the TacT toxicity (Figures 3A and 3B). The effects of these TacT mutations on the toxicity were also confirmed in an agar plate spotting assay.

These results, together with the previous toxicity assays using *Salmonella*, suggest that the base-specific hydrogen bonds observed in the present structure are important for the specific Gly-$tRNA^{Gly}$ acetylation by TacT.

U73 and G71 in $tRNA^{Gly}$ are required for acetylation by TacT

The structure of the TacT:AcGly-$tRNA^{Gly}$ complex suggested that TacT specifically recognizes the discriminator U73 and G71 of $tRNA^{Gly}$. The discriminator U73 is the most distinctive feature of $tRNA^{Gly}$, because only the $tRNA^{Gly}$ and $tRNA^{Cys}$ isoacceptors from *E. coli* and *Salmonella* have U73. However, $tRNA^{Cys}$ has C71, instead of G71. Therefore, the combination of U73 and G71, the unique sequence feature of $tRNA^{Gly}$, is recognized by TacT, which would thus discriminate $tRNA^{Gly}$ from other tRNA species for acetylation.

E. coli and *Salmonella* have three common $tRNA^{Gly}$ isoacceptors: $tRNA^{Gly}$GCC, $tRNA^{Gly}$CCC, and $tRNA^{Gly}$UCC (Figure 4A; Figure S1). All three Gly-$tRNA^{Gly}$s were efficiently acetylated by TacT to almost the same extent (Figures 4B and 4C), and the RNA sequences in the acceptor stems, recognized by TacT in the crystal structure, are conserved among the three $tRNA^{Gly}$ isoacceptors. We tested the acetylation of the mutant Gly-$tRNA^{Gly}$ by TacT *in vitro* (Figures 4B and 4C). The mutation of U73 to C73 or A73 drastically reduced the acetylation rate of Gly-$tRNA^{Gly}$ to the extent of less than 1% of wild-type Gly-$tRNA^{Gly}$, while the U73 to G73 mutation did not affect the acetylation rate (Figures 4B and 4C). Since the O6 and N1 atoms of G73 could interact with the main chain amide and the Oδ atom of Asn79, respectively, the Gly-$tRNA^{Gly}$ mutant with G73 was acetylated by TacT (Figures 4D and 4E). The mutation of C2-G71 to G2-C72 reduced the acetylation rate of Gly-$tRNA^{Gly}$ to the extent of around 10% of wild-type Gly-$tRNA^{Gly}$ (Figures 4B and 4C). On the other hand, the mutation of G4G5-C68C69 to C4C5-G68G69 did not reduce the acetylation rate by TacT significantly (Figures 4B and 4C), whereas it drastically reduced the acetylation rate by AtaT, which acetylates Gly-$tRNA^{Gly}$, Trp-$tRNA^{Trp}$, Phe-$tRNA^{Phe}$, Tyr-$tRNA^{Tyr}$, and Met-$tRNAf^{Met}$ by recognizing the consecutive G-C pairs in the bottom half of the acceptor stem (Yashiro et al., 2020) (Figure S4). Altogether, the discriminator U73 and the C2-G71 base pair in the acceptor stem are required for the efficient acetylation of Gly-$tRNA^{Gly}$ by TacT. These results are consistent with the specific interactions between TacT and $tRNA^{Gly}$ revealed in the crystal structure of the TacT:AcGly-$tRNA^{Gly}$ complex (Figure 2). The impact of the U73 mutation in $tRNA^{Gly}$ on the acetylation is larger than that of the mutation of G71 (Figures 4B and 4C). Thus, U73 is the most important base for $tRNA^{Gly}$ recognition by TacT, followed by G71, and the combination of U73 and G71 would increase the specificity of TacT toward $tRNA^{Gly}$.

Aminoacyl moiety binding site of TacT

In vitro acetylation assays of mutant Gly-$tRNA^{Gly}$ showed that Gly-$tRNA^{Gly}$ with G73, instead of U73, could be acetylated by TacT as efficiently as wild-type Gly-$tRNA^{Gly}$ (Figures 4B and

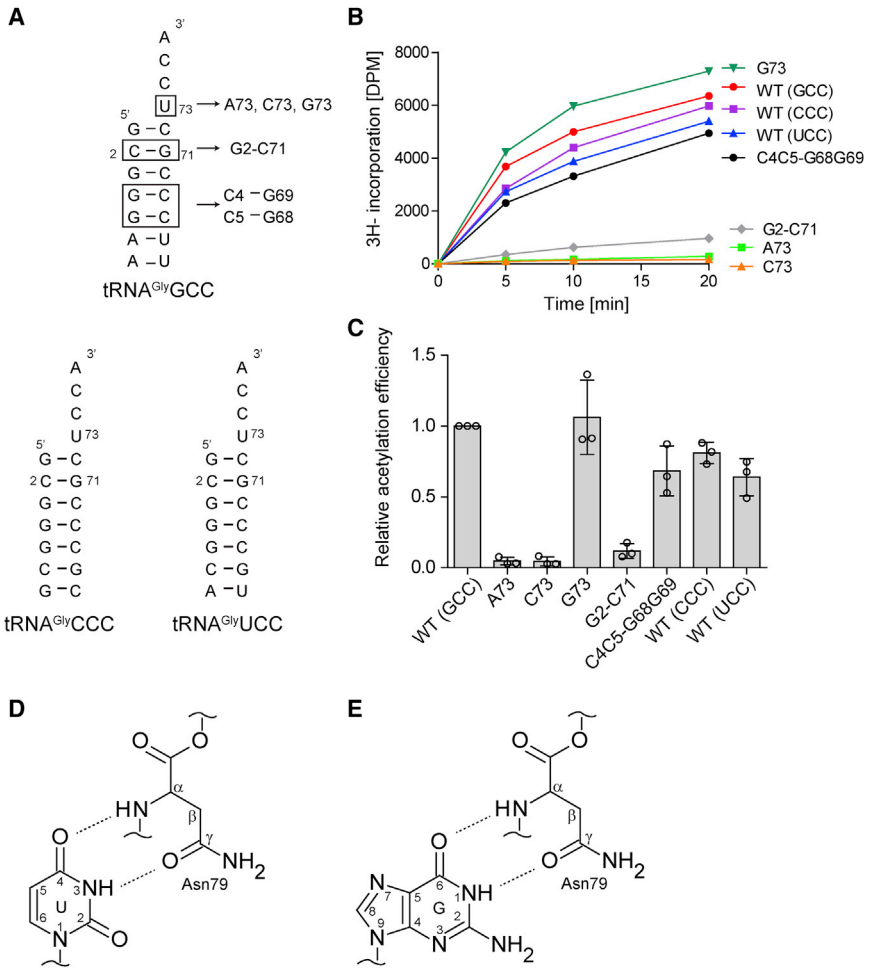

Figure 4. TacT recognition elements in tRNA^{Gly}

(A) Nucleotide sequences of acceptor helices of three tRNA^{Gly} isoacceptors: tRNA^{Gly}GCC, tRNA-^{Gly}CCC, and tRNA^{Gly}UCC. The nucleotide substitutions in the tRNA^{Gly}GCC transcripts used for assays in (B) are shown by boxes and arrows.

(B) Time courses of the acetylation of Gly-tRNA-^{Gly}GCC, Gly-tRNA^{Gly}CCC, Gly-tRNA^{Gly}UCC, and Gly-tRNA^{Gly}GCC variants (G2-C71, A73, C73, G73, and C4C5-G68G69) in (A).

(C) Relative acetylation rates of Gly-tRNA^{Gly} variants (10 μM) in (A) by TacT. The reaction mixtures were incubated for 5 min at 37°C, and the acetylation efficiency of Gly-tRNA^{Gly}GCC was taken as 1.0. The bars in the graph are SD of three independent (n = 3) experiments, and the data are presented as mean values ± SD.

(D) Interactions between U73 and Asn79 were observed in the structure of TacT:AcGly-tRNA^{Gly} complex.

(E) Possible interactions between G73 of tRNA and Asn79 of TacT.

4C). The combination of C2-G71 and U73 is the unique feature of tRNA^{Gly}, but tRNA^{Asn} and tRNA^{Arg}UCU of *E. coli* and *Salmonella* have C2-G71 and G73 (Figure 5A; Figure S1). Therefore, Asn-tRNA^{Asn} and Arg-tRNA^{Arg} might be acetylated by TacT. The acetylations of *E. coli* Asn-tRNA^{Asn} and Arg-tRNA^{Arg}UCU were tested *in vitro*, and the results showed that they were not significantly acetylated by TacT (Figure 5B), consistent with the *in vivo* analyses.

Furthermore, we transplanted the tRNA^{Gly} identity elements, C2-G71 and U73, for acetylation of Gly-tRNA^{Gly} by TacT, into tRNA^{Cys} (Figure 5C). tRNA^{Cys} also has U73 discriminator as tRNA^{Gly}, which is one of the main identity elements for the aminoacylation by cysteinyl-tRNA synthetase (CysRS) (McClain, 1993; Pallanck et al., 1992). tRNA^{Cys} variants with nucleotide replacement in the acceptor stem region are expected to be charged with Cys by CysRS and also be mischarged with Gly by glycyl-tRNA synthetase (GlyRS). As expected, tRNA^{Cys}(C2G3-C70G71) was charged with Cys by CysRS and also mischarged with Gly by GlyRS, while tRNA^{Cys} and tRNA^{Cys}(C2G71) were charged only with Cys by CysRS, *in vitro* (Figures 5D and 5E). Next, acetylation of these aminoacyl-tRNAs by TacT was tested *in vitro*. The results showed that neither Cys-tRNA^{Cys} nor Cys-tRNA^{Cys}(C2G71) nor Cys-tRNA^{Cys}(C2G3-C70G71) was acetylated by TacT (Figure 5F). On the other hand, Gly-charged tRNA^{Cys}(C2G3-C70G71), namely Gly-tRNA^{Cys}(C2G3-C70G71), was acetylated to almost the same extent as wild-type Gly-tRNA^{Gly} (Figure 5F). These results suggest that TacT would recognize not only the C2-G71 and U73 in tRNA substrate but also the aminoacyl moiety of aminoacyl-tRNAs.

In the present structure of the TacT:AcGly-tRNA complex, although the AcGly moiety was visible in one AcGly-tRNA^{Gly}, AcGly-A76 is directed in the opposite direction from the catalytic site of TacT (Figures 2B and 2C). This is because the structure represents the post-reaction stage, as described above. We manually modeled the aminoacyl moiety of Gly-tRNA^{Gly} in the catalytic pocket of TacT in the structure of the determined TacT:AcGly-tRNA^{Gly} complex (Figure 5G). In the model, the α-amino group of Gly in Gly-A76 of Gly-tRNA^{Gly} is close to the acetyl group of the modeled AcCoA in the catalytic pocket. The hydrophobic side chains of Val25, Leu26, and Leu132 and the main chain of Ala131 constitute a narrow gate, and the acetyl group of AcCoA is located behind the gate and the Gly of Gly-tRNA^{Gly} is at the gate entrance. This narrow gate would prevent the aminoacyl moiety of aminoacyl-tRNAs charged with bulky amino acids from accessing the catalytic site by steric hindrance. Thus, only aminoacyl-tRNAs charged with small amino acids can be accepted by TacT. This would explain why TacT excludes Asn-tRNA^{Asn} and Arg-tRNA^{Arg}UCU for acetylation, even though these tRNAs have the G73 and C2-G71 bases that can be recognized by TacT. It would also explain why neither mutant Cys-tRNA^{Cys}(C2G71) nor Cys-tRNA^{Cys} (C2G3-C70G71) was acetylated by TacT (Figure 5F). Consistent with this idea, the mutation of Leu26 to glutamate (L26E) reduced the TacT toxicity, and

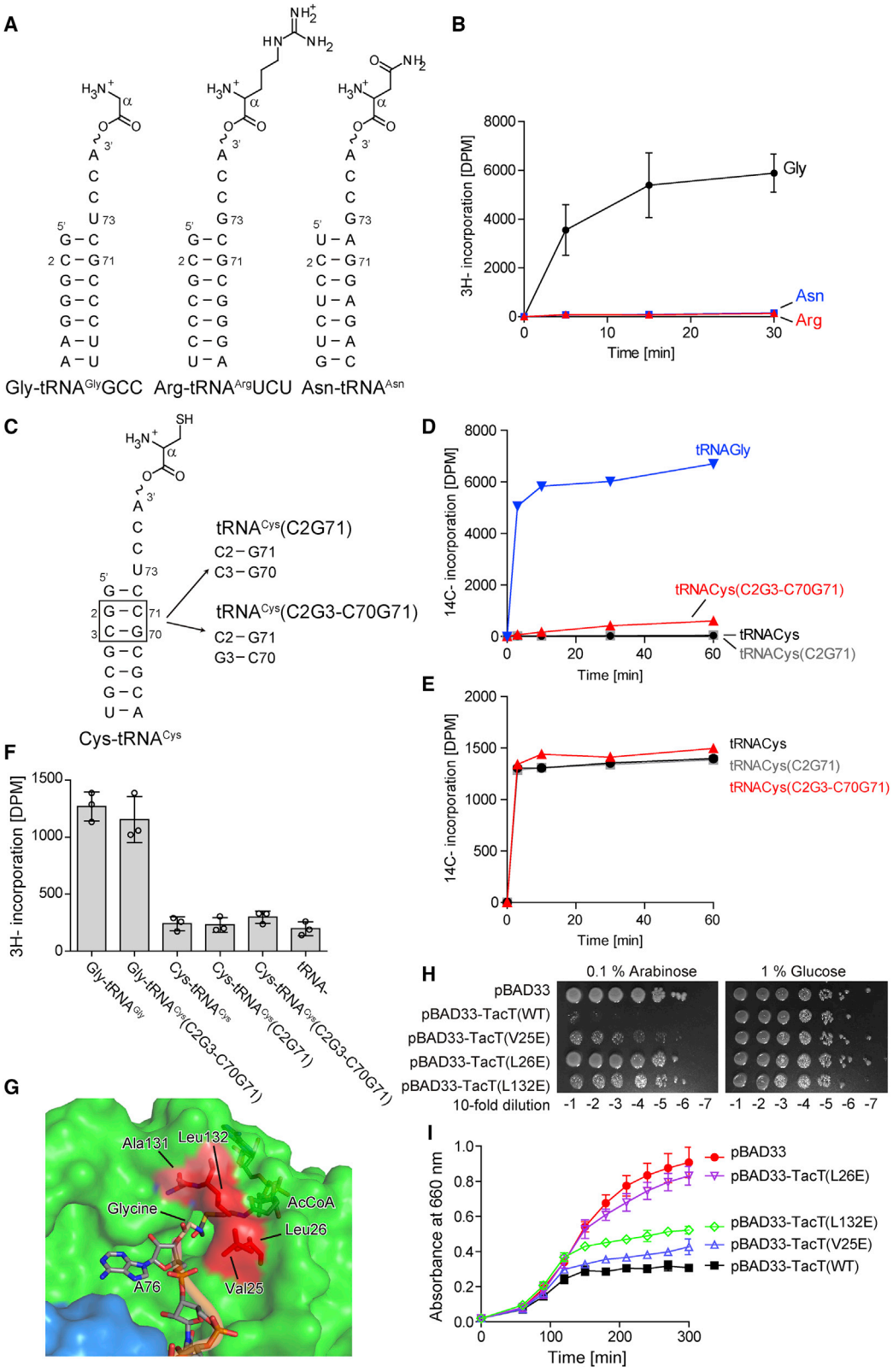

(legend on next page)

the V25E and L132E mutations also attenuated the TacT toxicity, in liquid and solid media (Figures 5H and 5I). Altogether, TacT would recognize both the size of the aminoacyl moiety of aminoacyl-tRNAs and the specific sequences in tRNA for the efficient acetylation of an aminoacyl-tRNA. Thus, TacT specifically and efficiently acetylates Gly-tRNA^{Gly}.

DISCUSSION

We have shown that Gly-tRNA^{Gly} is the only aminoacyl-tRNA acetylated by TacT *in vivo* (Figure 1C), and Gly-tRNA^{Gly} is most efficiently acetylated by TacT *in vitro* (Figures 1D and 1E). Consistent with these findings, the crystal structure of the TacT:AcGly-tRNA^{Gly} complex showed that TacT recognizes the unique features of tRNA^{Gly}: the discriminator U73 and G71 (Figure 2). Gly-tRNA^{Gly} with the U73G mutation and G71 is acetylated by TacT *in vitro* (Figures 4B and 4C); however, Asn-tRNA^{Asn} and Arg-tRNA^{Arg} with G73 and G71 were not acetylated *in vivo* and *in vitro* (Figures 1C and 5B). Furthermore, while neither Cys-tRNA^{Cys}(C2G71) nor Cys-tRNA^{Cys}(C2G3-C70G71) was acetylated, Gly-tRNA^{Cys}(C2G3-C70G71) was acetylated by TacT *in vitro* (Figure 5F). Thus, the present study suggests that TacT is a Gly-tRNA^{Gly}-specific acetyltransferase toxin, which recognizes the aminoacyl moiety of the aminoacyl-tRNA and the specific sequence in tRNA^{Gly}.

The mechanism of specific aminoacyl-tRNA selection by TacT would involve the following two consecutive or simultaneous reactions. The acceptor helixes of aminoacyl-tRNAs with U73/G73 and G71, Gly-tRNA^{Gly}, Asn-tRNA^{Asn}, and Arg-tRNA^{Arg} would bind to TacT. While the small 3′-Gly-moiety of Gly-RNA^{Gly} can enter the active site, neither the 3′-Asn-moiety of Asn-tRNA^{Asn} nor the 3′-Arg-moiety of Arg-tRNA^{Arg} can enter the active site, due to the larger size of the side chains of their aminoacyl moieties. Thus, Asn-tRNA^{Asn} and Arg-tRNA^{Arg} are rejected by TacT, and only Gly-tRNA^{Gly} is acetylated by TacT. In initial studies, TacT reportedly acetylated a variety of aminoacyl-tRNAs for Gly, Ile/Leu, Trp, and Ser, when TacT was added to an *in vitro* translation reaction (Cheverton et al., 2016; Rycroft et al., 2018). This promiscuous acetylation observed in the previous study (Rycroft et al., 2018) might be due to the *in vitro* conditions, where a relatively excessive amount of enzyme is incubated with aminoacyl-tRNAs until the reaction reaches a plateau.

The fundamental mechanism of the specific acetylation of Gly-tRNA^{Gly} by TacT is analogous to that of methionyl-tRNAf^{Met} transformylase (MTF). MTF catalyzes the formylation of α-amino group of initiator methionyl-tRNAf^{Met} specifically. The extensive biochemical and structural analyses of bacterial MTF showed that MTF recognizes the specific sequences found only in the initiator tRNAf^{Met}, C1-A72 mispair at the top of the acceptor stem and A11-G24 in the D-stem, as well as the methionyl-moiety of Met-tRNAf^{Met} (Guillon et al., 1992; Lee et al., 1991; Schmitt et al., 1998). Thus, TacT and MTF both recognize the specific nucleotides in the substrate aminoacyl-tRNAs as well as aminoacyl moieties and modify only the specific aminoacyl-tRNAs.

The AtaT2 encoded on the *E. coli* O157:H7 chromosome was recently suggested to be a Gly-tRNA^{Gly}-specific toxin (Ovchinnikov et al., 2020), while AtaT from *E. coli* O157:H7 acetylates Gly-tRNA^{Gly}, Trp-tRNA^{Trp}, Phe-tRNA^{Phe}, Tyr-tRNA^{Tyr}, and Met-tRNAf^{Met} *in vivo* and *in vitro* (Yashiro et al., 2020). In the report, ribosomal profiling in AtaT2-expressing *E. coli* cells showed that AtaT2 expression induces ribosome stalling on Gly codons in the A-site of the ribosome, and AtaT2 also acetylates Gly-tRNA^{Gly} *in vitro* (Ovchinnikov et al., 2020). However, the mechanism of the specific acetylation of Gly-tRNA^{Gly} by AtaT2 remained enigmatic. Our direct LC-MS analysis of acetylated aminoacyl-tRNAs in *E. coli* expressing AtaT2 demonstrated that Gly-tRNA^{Gly} was exclusively acetylated by AtaT2 *in vivo*, as TacT (Figure S5A), supporting the recent report. The amino acids in TacT that recognize the discriminator U73 and G71 of tRNA^{Gly} are conserved in AtaT2. We determined the crystal structure of AtaT2 in complex with its immunity AtaR2 (Table S1), which revealed that the structure of AtaT2 is homologous to that of TacT, and several key residues for the recognition of tRNA^{Gly} were aligned when the AtaT2 and TacT structures were superimposed (Figures S5B and S5C). Biochemical analyses of AtaT2 using Gly-tRNA^{Gly} variants as substrates showed that, like TacT, AtaT2 requires U73 and G71 for the efficient acetylation of Gly-tRNA^{Gly} (Figures S5D and S5E). Furthermore, the mutation of the amino acids in AtaT2, corresponding to those involved in the specific recognition of Gly-tRNA^{Gly} in TacT, suppressed

Figure 5. Recognition of aminoacyl moiety by TacT

(A) Nucleotide sequences of acceptor helices and aminoacyl moieties of Gly-tRNA^{Gly}GCC, Arg-tRNA^{Arg}UCU, and Ans-tRNA^{Asn}.

(B) Acetylation of Gly-tRNA^{Gly}GCC, Arg-tRNA^{Arg}UCU, and Asn-tRNA^{Asn} (10 μM) by TacT *in vitro*. The bars in the graph are SD of three independent (n = 3) experiments, and the data are presented as mean values ± SD.

(C) Nucleotide sequences of acceptor helices and aminoacyl moieties of wild-type Cys-tRNA^{Cys} and its variants, Cys-tRNA^{Cys} (C2G71) and Cys-tRNA^{Cys}(C2G3-C70G71).

(D) Time courses of glycylation of tRNA^{Gly}, wild-type tRNA^{Cys}, tRNA^{Cys}(C2G71), and tRNA^{Cys}(C2G3-C70G71) by GlyRS.

(E) Time courses of cysteinylation of wild-type tRNA^{Cys} and its variants by CysRS.

(F) Acetylation of Gly-tRNA^{Gly}, Cys-tRNA^{Cys} (wild type), Cys-tRNA^{Cys}(C2G71), Cys-tRNA^{Cys}(C2G3-C70G71), and Gly-tRNA^{Cys}(C2G3-C70G71) (2.2 μM) by TacT *in vitro*. The reaction mixtures were incubated for 3 min at 37°C. The bars in the graph are SD of three independent (n = 3) experiments, and the data are presented as mean values ± SD.

(G) Model of Gly-tRNA^{Gly} in the catalytic pocket of the TacT structure, shown as a surface model. Gly-tRNA^{Gly} and AcCoA are shown as stick models. The hydrophobic residues in the vicinity of the aminoacyl moiety of Gly-tRNA^{Gly} are colored red.

(H) Toxicity of TacT variants. Overnight cultures of *E. coli* MG1655 transformed with pBAD33-TacT and its variants were serially diluted, and the dilutions were spotted on LB agar plates containing 30 μg/mL chloramphenicol and supplemented with 0.1% (w/v) arabinose (left) or 1% (w/v) glucose (right). The plates were incubated at 37°C overnight.

(I) Growth curves of *E. coli* MG1655 transformed with pBAD33-TacT and its variants. *E. coli* MG1655 transformed by pBAD33-TacT or its variants in (H) was inoculated in LB containing 30 μg/mL chloramphenicol and 0.1% (w/v) arabinose and incubated at 37°C. Bars in the graphs indicate the SD of three independent (n = 3) experiments.

or attenuated the toxicity of AtaT2 *in vivo* (Figures S5F and S5G). Altogether, both AtaT2 and TacT are Gly-tRNA^{Gly}-specific acetyltransferase toxins that utilize the same mechanism for the selection of a specific aminoacyl-tRNA. In addition to C35 and C36 in the anticodon, the discriminator U73 and the C2-G71 base pair in tRNA^{Gly} are identity elements that contribute to the efficient glycylation of tRNA^{Gly} by *E. coli* GlyRS (Nameki et al., 1997). Thus, TacT may exploit the identity elements in the acceptor region of tRNA^{Gly} for the acetylation.

We recently reported that AtaT, another GNAT toxin identified in *E. coli* O157:H7, acetylates Gly-tRNA^{Gly}, Trp-tRNA^{Trp}, Phe-tRNA^{Phe}, Tyr-tRNA^{Tyr}, and Met-tRNAf^{Met} *in vivo* and *in vitro* (Yashiro et al., 2020). For the acetylation of aminoacyl-tRNAs by AtaT, both the consecutive G-C pairs in the bottom half of the tRNA acceptor stem and the aminoacyl moiety of aminoacyl-tRNAs are important. Although AtaT and TacT both share Gly-tRNA^{Gly} as a target for acetylation, they recognize different regions of tRNA^{Gly}: TacT recognizes U73 and G71 in the upper region of the acceptor of tRNA^{Gly}, and AtaT recognizes the consecutive G-C pairs in the bottom half of the acceptor stem of tRNA^{Gly}. Consistent with the fact that TacT and AtaT recognize different sites in the tRNAs for acetylation of the corresponding aminoacyl-tRNAs, the amino acid residues involved in tRNA recognition are not conserved between AtaT and TacT (Figure S5C). A superimposition of the structure of TacT:AcGly-tRNA^{Gly} complex with that of the AtaT:AcMet-tRNAf^{Met} complex (Yashiro et al., 2020) revealed that tRNA^{Gly} on TacT is rotated by approximately 60° on the acceptor helix axis, compared with tRNAf^{Met} bound to AtaT (Figure S6). Thus, the different tRNA-binding angles reflect that AtaT and TacT recognize different regions of the acceptor of aminoacyl-tRNAs.

Salmonella Typhimurium and *Salmonella* Enteritidis have three GNAT toxin genes, encoding TacT, TacT2, and TacT3 (Rycroft et al., 2018). The amino acid residues in TacT involved in the recognition of tRNA^{Gly} are conserved in TacT2, but not in TacT3 (Rycroft et al., 2018) (Figure S5C). Therefore, TacT2 would recognize and acetylate Gly-tRNA^{Gly} specifically, whereas TacT3 might recognize different aminoacyl-tRNAs from those of TacT and TacT2. The biological significance of the existence of GNAT toxins with the same specificity toward aminoacyl-tRNAs in *Salmonella* species is not well understood. TacT and TacT2 would function redundantly in the acetylation of Gly-tRNA^{Gly}, but the expression of TacT and TacT2 might be regulated differently under certain environmental conditions.

Understanding the functional mechanism of the toxins in the TA modules of pathogenetic bacteria is particularly important, from pathological and clinical viewpoints. Blocking the GNAT toxin activity in the persister cells is expected to restart their growth and restore the antibiotic susceptibility, leading to the prevention of the recalcitrance and relapse of bacterial infections. The molecular basis for the substrate specificity presented in this study will provide advanced information for the design of drugs targeting pathogenetic bacteria. To fully understand the mechanism and physiological activity of GNAT toxins, further characterizations of the acetylation targets and structural and biochemical analyses of the substrate recognition are awaited.

Limitations of the study

Specific acetylation of Gly-tRNA^{Gly} isoacceptors by TacT would reduce the amount of Gly-tRNA^{Gly} in cells and result in the inhibition of protein synthesis. As was reported for *E. coli* AtaT2, Gly-tRNA^{Gly}-specific GNAT toxin (Figure S5), the acetylation of Gly-tRNA^{Gly} induces the ribosome stalling at Gly codons in mRNAs and reduced the translation efficiencies of mRNAs containing Gly codons (Wilcox et al., 2018). Since the antitoxin against AtaT2, AtaR2, does not contain any Gly, it is assumed that the continuous AtaR2 synthesis during the AtaT2 expression constitutes negative feedback to prevent the excess AtaT2 expression and thus facilitate the recovery of cells from the toxin action. On the other hand, there is a Gly in *Salmonella* Typhimurium TacA antitoxin. Thus, it is unlikely that the specific acetylation of Gly-tRNA^{Gly} by TacT in *Salmonella* is for the negative feedback for the recovery from toxin action. The physiological significance of acetylation of specific aminoacyl-tRNA by GNAT toxins, including TacT, remains elusive. Furthermore, the biological relevance of specific aminoacyl-tRNA acetylation by TacT in the process of persister formation in macrophages remains enigmatic. Comprehensive analysis of mRNAs with reduced translation efficiency by the action of TacT in *Salmonella* might provide clues for the understanding of the regulatory mechanism of gene expression by TacT. This approach also provides insights into the significance of specific aminoacyl-tRNA acetylation by TacT in persister formation of *Salmonella* Typhimurium in macrophages.

STAR★METHODS

Detailed methods are provided in the online version of this paper and include the following:

- KEY RESOURCES TABLE
- RESOURCE AVAILABILITY
  - Lead contact
  - Materials availability
  - Data and code availability
- EXPERIMENTAL MODEL AND SUBJECT DETAILS
  - Bacterial cells
- METHOD DETAILS
  - Construction of plasmids
  - Overexpression and purification of proteins
  - LC/MS analysis of acetylated aminoacyl-tRNAs upon TacT expression in *E. coli*
  - Purification of overexpressed tRNAs in *E. coli*
  - *In vitro* acetylation assay
  - Crystallization and structure determination of TacT complexed with acetyl Gly-tRNA^{Gly}
  - Crystallization and structure determination of AtaT2-AtaR2 complex
  - *In vitro* transcription of tRNAs
  - *In vivo* toxicity assay for TacT, AtaT2, and their variants
- QUANTIFICATION AND STATISTICAL ANALYSIS

SUPPLEMENTAL INFORMATION

Supplemental information can be found online at https://doi.org/10.1016/j.celrep.2021.110130.

ACKNOWLEDGMENTS

We thank the beamline staff of BL-17A (KEK, Tsukuba) for technical assistance during data collection. This work was supported by a Grant-in-Aid for Scientific Research (18H03980 to K.T., 18H05272 to T.S.), a Grant-in-Aid for Early-Career Scientists (19K16069 to Y.Y.), and a Grant-in-Aid for Scientific Research on Innovative Areas (26113002 to K.T.) from JSPS; an Exploratory Research for Advanced Technology grant (ERATO, JPMJER2002 to T.S.) from JST; and grants (to K.T.) from The Japan Foundation for Applied Enzymology, The Toyo Suisan Foundation, The Tojuro Iijima Foundation for Food Science and Technology, The Naito Foundation, and The Takahashi Industrial and Economic Research Foundation.

AUTHOR CONTRIBUTIONS

K.T. planned and designed the research, and Y.Y. performed the protein and RNA preparation, crystallization, structure determination, and biochemical and functional analyses. C.Z. performed protein purification and crystallization. Y.S. and T.S. assisted with the LC-MS spectrometric analysis. Y.Y. and K.T. analyzed the data and wrote the paper.

DECLARATION OF INTERESTS

The authors declare no competing interests.

Received: August 10, 2021
Revised: October 25, 2021
Accepted: November 23, 2021
Published: December 21, 2021

REFERENCES

Afonine, P.V., Grosse-Kunstleve, R.W., Echols, N., Headd, J.J., Moriarty, N.W., Mustyakimov, M., Terwilliger, T.C., Urzhumtsev, A., Zwart, P.H., and Adams, P.D. (2012). Towards automated crystallographic structure refinement with phenix.refine. Acta Crystallogr. D Biol. Crystallogr. *68*, 352–367.

Balaban, N.Q., Merrin, J., Chait, R., Kowalik, L., and Leibler, S. (2004). Bacterial persistence as a phenotypic switch. Science *305*, 1622–1625.

Byrne, R.T., Konevega, A.L., Rodnina, M.V., and Antson, A.A. (2010). The crystal structure of unmodified tRNAPhe from Escherichia coli. Nucleic Acids Res. *38*, 4154–4162.

Chan, P.P., and Lowe, T.M. (2016). GtRNAdb 2.0: an expanded database of transfer RNA genes identified in complete and draft genomes. Nucleic Acids Res. *44* (*D1*), D184–D189.

Cheverton, A.M., Gollan, B., Przydacz, M., Wong, C.T., Mylona, A., Hare, S.A., and Helaine, S. (2016). A Salmonella Toxin Promotes Persister Formation through Acetylation of tRNA. Mol. Cell *63*, 86–96.

Chung, H.S., and Raetz, C.R.H. (2010). Interchangeable domains in the Kdo transferases of Escherichia coli and Haemophilus influenzae. Biochemistry *49*, 4126–4137.

Emsley, P., Lohkamp, B., Scott, W.G., and Cowtan, K. (2010). Features and development of Coot. Acta Crystallogr. D Biol. Crystallogr. *66*, 486–501.

Gerdes, K., Bech, F.W., Jørgensen, S.T., Løbner-Olesen, A., Rasmussen, P.B., Atlung, T., Boe, L., Karlstrom, O., Molin, S., and von Meyenburg, K. (1986). Mechanism of postsegregational killing by the hok gene product of the parB system of plasmid R1 and its homology with the relF gene product of the E. coli relB operon. EMBO J. *5*, 2023–2029.

Goeders, N., and Van Melderen, L. (2014). Toxin-antitoxin systems as multilevel interaction systems. Toxins (Basel) *6*, 304–324.

Guillon, J.M., Meinnel, T., Mechulam, Y., Lazennec, C., Blanquet, S., and Fayat, G. (1992). Nucleotides of tRNA governing the specificity of Escherichia coli methionyl-tRNA(fMet) formyltransferase. J. Mol. Biol. *224*, 359–367.

Harms, A., Maisonneuve, E., and Gerdes, K. (2016). Mechanisms of bacterial persistence during stress and antibiotic exposure. Science *354*, 9.

Harms, A., Brodersen, D.E., Mitarai, N., and Gerdes, K. (2018). Toxins, Targets, and Triggers: An Overview of Toxin-Antitoxin Biology. Mol. Cell *70*, 768–784.

Hayes, F., and Van Melderen, L. (2011). Toxins-antitoxins: diversity, evolution and function. Crit. Rev. Biochem. Mol. Biol. *46*, 386–408.

Helaine, S., and Kugelberg, E. (2014). Bacterial persisters: formation, eradication, and experimental systems. Trends Microbiol. *22*, 417–424.

Helaine, S., Cheverton, A.M., Watson, K.G., Faure, L.M., Matthews, S.A., and Holden, D.W. (2014). Internalization of Salmonella by macrophages induces formation of nonreplicating persisters. Science *343*, 204–208.

Hentzen, D., Mandel, P., and Garel, J.P. (1972). Relation between aminoacyl-tRNA stability and the fixed amino acid. Biochim. Biophys. Acta *281*, 228–232.

Jühling, F., Mörl, M., Hartmann, R.K., Sprinzl, M., Stadler, P.F., and Pütz, J. (2009). tRNAdb 2009: compilation of tRNA sequences and tRNA genes. Nucleic Acids Res. *37*, D159–D162.

Jurėnas, D., Chatterjee, S., Konijnenberg, A., Sobott, F., Droogmans, L., Garcia-Pino, A., and Van Melderen, L. (2017a). AtaT blocks translation initiation by N-acetylation of the initiator tRNA^{fMet}. Nat. Chem. Biol. *13*, 640–646.

Jurėnas, D., Garcia-Pino, A., and Van Melderen, L. (2017b). Novel toxins from type II toxin-antitoxin systems with acetyltransferase activity. Plasmid *93*, 30–35.

Kabsch, W. (2010). XDS. Acta Crystallogr. D Biol. Crystallogr. *66*, 125–132.

Lee, C.P., Seong, B.L., and RajBhandary, U.L. (1991). Structural and sequence elements important for recognition of Escherichia coli formylmethionine tRNA by methionyl-tRNA transformylase are clustered in the acceptor stem. J. Biol. Chem. *266*, 18012–18017.

Maisonneuve, E., and Gerdes, K. (2014). Molecular mechanisms underlying bacterial persisters. Cell *157*, 539–548.

McClain, W.H. (1993). Identity of Escherichia coli tRNA(Cys) determined by nucleotides in three regions of tRNA tertiary structure. J. Biol. Chem. *268*, 19398–19402.

McCoy, A.J., Grosse-Kunstleve, R.W., Adams, P.D., Winn, M.D., Storoni, L.C., and Read, R.J. (2007). Phaser crystallographic software. J. Appl. Cryst. *40*, 658–674.

McVicker, G., and Tang, C.M. (2016). Deletion of toxin-antitoxin systems in the evolution of Shigella sonnei as a host-adapted pathogen. Nat. Microbiol. *2*, 16204–16211.

Meinnel, T., and Blanquet, S. (1995). Maturation of pre-tRNA(fMet) by Escherichia coli RNase P is specified by a guanosine of the 5′-flanking sequence. J. Biol. Chem. *270*, 15908–15914.

Mulcahy, L.R., Burns, J.L., Lory, S., and Lewis, K. (2010). Emergence of Pseudomonas aeruginosa strains producing high levels of persister cells in patients with cystic fibrosis. J. Bacteriol. *192*, 6191–6199.

Muthuramalingam, M., White, J.C., and Bourne, C.R. (2016). Toxin-Antitoxin Modules Are Pliable Switches Activated by Multiple Protease Pathways. Toxins (Basel) *8*, 16.

Nameki, N., Tamura, K., Asahara, H., and Hasegawa, T. (1997). Recognition of tRNAGly by three widely diverged glycyl-tRNA synthetases. J. Mol. Biol. *268*, 640–647.

Ovchinnikov, S.V., Bikmetov, D., Livenskyi, A., Serebryakova, M., Wilcox, B., Mangano, K., Shiriaev, D.I., Osterman, I.A., Sergiev, P.V., Borukhov, S., et al. (2020). Mechanism of translation inhibition by type II GNAT toxin AtaT2. Nucleic Acids Res. *48*, 8617–8625.

Page, R., and Peti, W. (2016). Toxin-antitoxin systems in bacterial growth arrest and persistence. Nat. Chem. Biol. *12*, 208–214.

Pallanck, L., Li, S., and Schulman, L.H. (1992). The anticodon and discriminator base are major determinants of cysteine tRNA identity in vivo. J. Biol. Chem. *267*, 7221–7223.

Pandey, D.P., and Gerdes, K. (2005). Toxin-antitoxin loci are highly abundant in free-living but lost from host-associated prokaryotes. Nucleic Acids Res. *33*, 966–976.

Qian, H., Yao, Q., Tai, C., Deng, Z., Gan, J., and Ou, H.Y. (2018). Identification and characterization of acetyltransferase-type toxin-antitoxin locus in Klebsiella pneumoniae. Mol. Microbiol. *108*, 336–349.

Rycroft, J.A., Gollan, B., Grabe, G.J., Hall, A., Cheverton, A.M., Larrouy-Maumus, G., Hare, S.A., and Helaine, S. (2018). Activity of acetyltransferase toxins involved in Salmonella persister formation during macrophage infection. Nat. Commun. *9*, 1993.

Schmitt, E., Panvert, M., Blanquet, S., and Mechulam, Y. (1998). Crystal structure of methionyl-tRNAfMet transformylase complexed with the initiator formyl-methionyl-tRNAfMet. EMBO J. *17*, 6819–6826.

Strong, M., Sawaya, M.R., Wang, S., Phillips, M., Cascio, D., and Eisenberg, D. (2006). Toward the structural genomics of complexes: crystal structure of a PE/PPE protein complex from Mycobacterium tuberculosis. Proc. Natl. Acad. Sci. USA *103*, 8060–8065.

Walker, S.E., and Fredrick, K. (2008). Preparation and evaluation of acylated tRNAs. Methods *44*, 81–86.

Waterhouse, A., Bertoni, M., Bienert, S., Studer, G., Tauriello, G., Gumienny, R., Heer, F.T., de Beer, T.A.P., Rempfer, C., Bordoli, L., et al. (2018). SWISS-MODEL: homology modelling of protein structures and complexes. Nucleic Acids Res. *46* (*W1*), W296–W303.

Wilcox, B., Osterman, I., Serebryakova, M., Lukyanov, D., Komarova, E., Gollan, B., Morozova, N., Wolf, Y.I., Makarova, K.S., Helaine, S., et al. (2018). Escherichia coli ItaT is a type II toxin that inhibits translation by acetylating isoleucyl-tRNAIle. Nucleic Acids Res. *46*, 7873–7885.

Yamaguchi, Y., and Inouye, M. (2011). Regulation of growth and death in Escherichia coli by toxin-antitoxin systems. Nat. Rev. Microbiol. *9*, 779–790.

Yang, Z., Ebright, Y.W., Yu, B., and Chen, X. (2006). HEN1 recognizes 21-24 nt small RNA duplexes and deposits a methyl group onto the 2′ OH of the 3′ terminal nucleotide. Nucleic Acids Res. *34*, 667–675.

Yashiro, Y., Yamashita, S., and Tomita, K. (2019). Crystal Structure of the Enterohemorrhagic Escherichia coli AtaT-AtaR Toxin-Antitoxin Complex. Structure *27*, 476–484.e3.

Yashiro, Y., Sakaguchi, Y., Suzuki, T., and Tomita, K. (2020). Mechanism of aminoacyl-tRNA acetylation by an aminoacyl-tRNA acetyltransferase AtaT from enterohemorrhagic E. coli. Nat. Commun. *11*, 5438.

Yeo, C.C. (2018). GNAT toxins of bacterial toxin-antitoxin systems: acetylation of charged tRNAs to inhibit translation. Mol. Microbiol. *108*, 331–335.

Zhang, C., Yashiro, Y., Sakaguchi, Y., Suzuki, T., and Tomita, K. (2020). Substrate specificities of Escherichia coli ItaT that acetylates aminoacyl-tRNAs. Nucleic Acids Res. *48*, 7532–7544.

STAR★METHODS

KEY RESOURCES TABLE

REAGENT or RESOURCE	SOURCE	IDENTIFIER
Bacterial and virus strains		
E. coli BL21(DE3)	Novagen	Cat#69450-3CN
E. coli MG1655	NBRP: *E. coli*	ME7986
Chemicals, peptides, and recombinant proteins		
Ni-NTA agarose	QIAGEN	Cat#30210
HiTrap Heparin, 5mL	GE Healthcare	Cat#17-0407-01
HiLoad 16/60 Superdex 200 PG	GE Healthcare	Cat#17-1069-01
Superdex 200 Increase 10/300 GL	GE Healthcare	Cat#28-9909-44
Resource Q, 6 mL	GE Healthcare	Cat#17-1179-01
Delta Pak C4 Prep Column	Waters	WAT011813
Deposited data		
TacT complexed with AcGly-tRNA^{Gly}	This study	PDB: 7F36 (https://doi.org/10.2210/pdb7f36/pdb)
AtaT2-AtaR2 structure	This study	PDB: 7F37, (https://doi.org/10.2210/pdb7f37/pdb)
Crystal structure of TacT from *Salmonella*	Cheverton et al., 2016	PDB: 5FVJ (https://doi.org/10.2210/pdb5fvj/pdb)
Crystal structure of unmodified *E. coli* tRNA^{Phe}	Byrne et al., 2010	PDB: 3L0U (https://doi.org/10.2210/pdb3l0u/pdb)
Structure of Conserved Putative Transcriptional Factor from *Vibrio cholerae* O1 biovar eltor str. N16961		PDB: 1Y9B, (https://doi.org/10.2210/pdb1y9b/pdb)
Oligonucleotides		
Primers for PCR, see Table S3	This study	N/A
Recombinant DNA		
pET-22b (+)	Novagen	Cat#69744-3CN
pBAD33.1	Chung and Raetz, 2010	Addgene #36267
Synthetic tacAT operon gene, see Table S2	This study	N/A
Synthetic tacT(Y140F) gene, see Table S2	This study	N/A
Synthetic ataR2T2 operon gene, see Table S2	This study	N/A
Synthetic tRNA^{Gly} template for T7 transcription, see Table S2	This study	N/A
Synthetic tRNA^{Gly} variant template for T7 transcription, see Table S2	This study	N/A
Synthetic tRNA^{Arg}UCU template for T7 transcription, see Table S2	This study	N/A
Synthetic tRNA^{Asn} template for T7 transcription, see Table S2	This study	N/A
Synthetic tRNA^{Cys} template for T7 transcription, see Table S2	This study	N/A
Synthetic tRNA^{Cys} variant template for T7 transcription, see Table S2	This study	N/A
Software and algorithms		
XDS	Kabsch, 2010	https://xds.mr.mpg.de/

(*Continued on next page*)

Continued

REAGENT or RESOURCE	SOURCE	IDENTIFIER
Phaser	McCoy et al., 2007	https://www-structmed.cimr.cam.ac.uk/phaser_obsolete/
Phenix	Afonine et al., 2012	https://phenix-online.org/
Swiss-Model	Waterhouse et al., 2018	https://swissmodel.expasy.org/
Coot	Emsley et al., 2010	https://www2.mrc-lmb.cam.ac.uk/personal/pemsley/coot/

RESOURCE AVAILABILITY

Lead contact

Further information and requests for resources and reagents should be directed to the lead contact, Kozo Tomita (kozo-tomita@edu.k.u-tokyo.ac.jp).

Materials availability

All unique reagents generated in this study will be available from the lead contact upon request without restrictions.

Data and code availability

- Coordinates and structure factors of the structures of the TacT:AcGly-tRNA^{Gly} complex and the AtaT2-AtaR2 complex have been deposited in the Protein Data Bank and are publicly available as of the data of publication. Accession codes are listed in the key resources table.
- This paper does not report original code.
- Any additional information required to reanalyze the data reported in this paper is available from the lead contact upon request.

EXPERIMENTAL MODEL AND SUBJECT DETAILS

Bacterial cells

We used *E. coli* BL21 (DE3) cells to produce all recombinant proteins used in this study and *E. coli* MG1655 to test the toxicity of toxins. The cells were cultured in LB media at 37°C.

METHOD DETAILS

Construction of plasmids

Synthetic DNAs encoding the toxin-antitoxin modules, *tacAT* and *ataR2T2,* and the catalytic mutants of the toxins, *tacT*(Y140F) and *ataT2*(Y139A), were purchased from Eurofins, Japan. The nucleotide sequences of the synthetic DNAs are listed in Table S2. For overexpression of TacA-TacT and the AtaR2-AtaT2 complex, the *tacAT* or *ataR2T2* module was PCR amplified and cloned between the *Nde*I and *Xho*I sites of pET22b, yielding pET22-TacAT and pET22-AtaR2T2, respectively. For the expression of catalytically inactive TacT(Y140F) and AtaT2(Y139A), the DNA fragment encoding *TacT*(Y140F) or *AtaT2*(Y139A) was PCR amplified and cloned between the *Nde*I and *Xho*I sites of pET22b, yielding pET22-TacT(Y140F) and pET22-AtaT2(Y139A), respectively. For toxicity analyses of TacT and AtaT2 in *E. coli*, the DNA fragment encoding *tacT* or *ataT2* was PCR amplified from pET22-TacAT or pET22-AtaR2T2 and cloned between the *Nde*I and HindIII sites of pBAD33.1 (Chung and Raetz, 2010), yielding pBAD33-TacT and pBAD33-AtaT2, respectively. pBAD33-TacT and pBAD33-AtaT2 have the 5′-CATAGCTAGCT-3′ sequence, which was introduced in the plasmids during the cloning, upstream of their *Nde*I sites. Mutations in pBAD33-TacT and pBAD33-AtaT2 were introduced by PCR. The plasmids for the expression of isoleucyl-tRNA synthetase and glutaminyl-tRNA synthetase were described previously (Yashiro et al., 2020; Zhang et al., 2020). The plasmids for the overexpression of other aminoacyl-tRNA synthetases (ARSs: AlaRS, LeuRS, GlyRS, TrpRS, SerRS, CysRS, ArgRS, AsnRS, and PheRS) were kind gifts from Dr. Shimizu (RIKEN, Japan). The oligonucleotide sequences used for the plasmid constructions and mutagenesis are listed in Table S3.

Overexpression and purification of proteins

For the expression of TacT(Y140F), AtaT2(Y139A), the TacA-TacT complex, and the AtaR2-AtaT2 complex, *E. coli* BL21(DE3) cells were transformed by pET22-TacT(Y140F), pET22-AtaT2(Y139A), pET22-TacAT, and pET22-AtaR2T2, respectively, inoculated in LB containing 50 μg/ml ampicillin, and cultured at 37°C until the OD_{600} reached ~0.8. Protein expression was induced by adding 0.1 mM IPTG, and the cultures were continued at 20°C for 16 hours. The cells were harvested and sonicated in buffer containing 25 mM Tris-Cl, pH 7.0, 500 mM NaCl, 20 mM imidazole, 5 mM β-mercaptoethanol, and 5% (v/v) glycerol. The lysates were centrifuged and the

clear supernatants were applied to Ni-NTA columns (QIAGEN, Japan), which were washed with buffer containing 25 mM Tris-Cl, pH 7.0, 500 mM NaCl, 20 mM imidazole, 5 mM β-mercaptoethanol, and 5% (v/v) glycerol. The proteins were eluted from the columns with buffer containing 25 mM Tris-Cl, pH 7.0, 500 mM NaCl, 400 mM imidazole, 5 mM β-mercaptoethanol, and 5% (v/v) glycerol. The proteins were separated on a Hi-Trap Heparin column (GE Healthcare, Japan) using a gradient of NaCl (100 - 1,000 mM) in buffer containing 25 mM Tris-Cl, pH 7.0, with 10 mM β-mercaptoethanol. The fractions containing proteins were pooled and finally separated by chromatography on a Superdex 200 column (GE Healthcare, Japan), in buffer containing 25 mM Tris-Cl, pH 7.0, 200 mM NaCl, and 10 mM β-mercaptoethanol. The proteins were concentrated and stored at −80°C. TacT and AtaT2 were prepared from their toxin-antitoxin complexes. The TacA-TacT or AtaR2-AtaT2 complex, purified as described above, was denatured in buffer containing 20 mM Tris-Cl, pH 8.0, 500 mM NaCl, 20 mM imidazole, and 8 M urea. The protein solution was applied onto the Ni-NTA column, which was washed with buffer containing 20 mM Tris-Cl, pH 8.0, 500 mM NaCl, 20 mM imidazole, and 8 M urea (Yashiro et al., 2019, 2020; Zhang et al., 2020). Antitoxins were removed in the eluate, and the histidine-tagged TacT or AtaT2 was retained on the column. TacT was refolded on the column with stepwise concentrations of urea (6 M, 4 M, 2 M, 1 M, 0.5 M, and 0 M), and eluted from the column with buffer containing 50 mM Tris-Cl, pH 7.0, 500 mM NaCl, 10 mM β-mercaptoethanol, 10% (v/v) glycerol, and 400 mM imidazole. The refolded TacT was further purified on a HiTrap Heparin column, as described above. For the refolding, AtaT2 was eluted from the column with buffer containing 20 mM Tris-Cl, pH 8.0, 500 mM NaCl, 400 mM imidazole, and 8 M urea, and refolded by dialysis against buffer containing 20 mM Tris-Cl, pH 7.0, 250 mM NaCl, 5% (v/v) glycerol and 1 mM DTT, at 4°C for 16 hours. The proteins were concentrated and stored at −80°C. The *E. coli* aminoacyl-tRNA synthetases (ARSs) used in this study were overexpressed in *E. coli* BL21(DE3), and purified by chromatography on Ni-NTA and HiTrap Heparin columns. Finally, the ARSs were purified on a HiLoad 16/60 Superdex 200 column, in buffer containing 20 mM Tris-HCl, pH 7.0, 200 mM NaCl, and 10 mM β-mercaptoethanol, as described previously (Yashiro et al., 2020; Zhang et al., 2020).

LC/MS analysis of acetylated aminoacyl-tRNAs upon TacT expression in *E. coli*

E. coli strain MG1655, purchased from NBRP: *E. coli* (NIG, Japan; ME7986), was transformed with pBAD33-TacT (or pBAD-AtaT2) or empty pBAD33 and cultured overnight. The overnight cultures were diluted to an OD_{660} of 0.02 in fresh liquid LB (4 ml) containing 30 μg/ml chloramphenicol, and cultured at 37°C until the OD_{660} reached 0.3. Then, 0.02% (w/v) arabinose was added to induce TacT (or AtaT2) expression. Cells were harvested at 10, 30, and 60 min after the induction. The cells were suspended in buffer containing 50 mM NaOAc, pH 5.0, 0.5 mM EDTA and 0.2 M NaCl and the RNA was extracted by phenol saturated with 300 mM NaOAc, pH 5.2. Acetylation of the α-amino group of the aminoacyl moiety of aminoacyl-tRNAs (aa-tRNAs) stabilizes the aminoacyl bonds (Hentzen et al., 1972). Under neutral or lower pH conditions, acetylated aa-tRNAs are hardly deacylated. Thus, under the acidic and lower temperature conditions used in the preparation of aa-tRNA and Ac-aa-tRNA from *E. coli* with induction of TacT expression, neither aa-tRNA nor Ac-aa-tRNA is ever deacylated. Thus, the quantitative analyses of the *in vivo* substrate specificity of TacT are not affected by the differences of the half-lives of Ac-aa-tRNA. The prepared fractions containing aa-tRNAs and Ac-aa-tRNAs acetylated by TacT (or AtaT2), as described above, were treated with acetic anhydride-D6 (Sigma, Japan), to convert the aa-tRNAs, which were not acetylated by TacT (or AtaT2) *in vivo*, to Ac(D3)-aa-tRNAs (Walker and Fredrick, 2008). The Ac-aa-tRNAs and Ac(D3)-aa-tRNAs were digested with RNase One Ribonuclease (Promega, Japan), in a reaction mixture (25 μL volume) containing 25 mM NH_4OAc and 2.5 units enzyme, at 37°C for 60 min. The digests were subjected to an LC/MS analysis using a Q Exactive Hybrid Quadrupole-Orbitrap Mass Spectrometer (Thermo Fisher Scientific), equipped with a Dionex UltiMate 3000 LC System (Thermo Fisher Scientific) and an InertSustain C18 column (5 μm, 2.1 × 250 mm, GL Sciences). Elution was performed with a multi-linear gradient, as described (Yashiro et al., 2019, 2020; Zhang et al., 2020).

Purification of overexpressed tRNAs in *E. coli*

For overexpression of $tRNA^{Ser}$ and $tRNA^{Cys}$, the synthetic DNA fragments encoding the *E. coli* $tRNA^{Ser}$ and $tRNA^{Cys}$ genes were PCR amplified and inserted between the *Sac*I and PstI sites of the pBSTNAV3 plasmid (Guillon et al., 1992). DNA fragment sequences are listed in Table S3. The pBSTNAV3 plasmids expressing $tRNA^{Gly}GCC$, $tRNA^{Ala}$, $tRNA^{Ile}$, $tRNA^{Leu}$, $tRNA^{Trp}$, $tRNA^{Phe}$, and $tRNA^{Gln}$ were described previously (Yashiro et al., 2020). tRNAs were overexpressed in the *E. coli* JM101Tr strain and purified as described (Guillon et al., 1992; Meinnel and Blanquet, 1995). The tRNA fractions enriched with the overexpressed tRNA were aminoacylated by their cognate aminoacyl-tRNA synthetases, and the amounts of the enriched isoacceptor tRNAs were measured.

In vitro acetylation assay

tRNA was first aminoacylated in a mixture containing 20 mM Tris-HCl, pH 7.4, 150 mM KCl, 7 mM $MgCl_2$, 10 mM β-mercaptoethanol, 15 μM tRNA, 1 mM glycine, and 2 μM GlyRS, at 37°C for 60 min. The acetylation reaction was started by adding [acetyl-^{3}H] Coenzyme A (10 Ci $mmol^{-1}$, Perkin Elmer, Japan) and TacT to final concentrations of 133 μM and 40 nM, respectively. In the case of AtaT2, it was added to a final concentration of 5 nM. The final concentration of aminoacyl-tRNA in the acetylation reaction mixture was adjusted to 10 μM. An aliquot of the reaction was spotted onto a Whatman 3MM filter (Whatman, Japan) and the radioactivities on the filters were measured with a liquid scintillation counter (Hitachi Aloka Medical, Japan). For the acetylation of wild-type and variant $tRNA^{Cys}$ charged with cysteine or glycine, the final concentration of aminoacyl-tRNA in the reaction mixture was adjusted to 2.2 μM based on the cysteine and glycine acceptance measured using [1,2,1',2'-^{14}C] L-Cystine (200 mCi/mmol, Perkin Elmer) and [1-^{14}C] Glycine (110 mCi/mmol, ARC). tRNAs were aminoacylated in a mixture containing 20 mM Tris-HCl, pH 7.4, 150 mM KCl, 7 mM $MgCl_2$, 1 mM DTT, 1 mM cysteine

or glycine, and 2 μM CysRS or GlyRS. The acetylation reaction was started by adding [acetyl-^{3}H] Coenzyme A (10 Ci mmol-1, Perkin Elmer, Japan) and TacT to final concentrations of 133 μM and 80 nM, respectively, and incubated at 37°C for 3 min.

Crystallization and structure determination of TacT complexed with acetyl Gly-tRNA^{Gly}

The tRNA^{Gly} fraction purified from *E. coli* overexpressing tRNA^{Gly}GCC, as described above, was further separated on a Delta Pak C4 Prep Column, with a 15 μm endcap and a 300 Å pore size (Waters, Japan), by a linear methanol gradient (0 - 48 %) in buffer containing 400 mM NaCl, 10 mM MgOAc, and 20 mM NH_4OAc, pH 5.2. The purified tRNA^{Gly} was aminoacylated by GlyRS, in a reaction mixture containing 20 mM Tris-HCl, pH 7.4, 150 mM KCl, 7 mM $MgCl_2$, 10 mM β-mercaptoethanol, 10 A_{260}/ml tRNA^{Gly}, 10 mM glycine, 2 mM ATP, and 0.4 μM GlyRS, at 37°C for 1 hour. The reaction product was extracted by cold phenol saturated with 300 mM NaOAc, pH 5.2, and applied to a NAP-5 column (GE Healthcare, Japan) at 4°C to remove the remaining ATP. The Gly-tRNA^{Gly} recovered by isopropanol precipitation was dissolved in 600 μL of 0.3 M NaOAc, pH 5.2, chemically acetylated by adding 30 μL of acetic anhydride, and incubated for 15 min on ice (Walker and Fredrick, 2008). The acetic anhydride addition and incubation were repeated four times. The reaction mixture was then ethanol precipitated and separated on a Delta Pak C4 Prep Column (Waters, Japan), as described above.

For crystallization, a mixture of 40 μM TacT (Y140F) protein and 44 μM acetyl Gly-tRNA^{Gly} was incubated on ice for 30 min, in buffer containing 10 mM Tris-HCl, pH 7.0, 100 mM NaCl, and 5 mM β-mercaptoethanol. Afterward, 0.2 μL of the mixture was mixed with 0.2 μL of reservoir solution, containing 200 mM calcium acetate, 100 mM sodium cacodylate, pH 6.0, 14% (v/v) PEG 8000, and crystals were generated by the sitting drop vapor diffusion method at 20°C.

Datasets were collected at beamline 17A at the Photon Factory at KEK, Japan. The crystals were flash-cooled in 1.1 × concentrated reservoir solution, supplemented with 20% (v/v) ethylene glycol as a cryoprotectant. The data were indexed, integrated, and scaled with XDS (Kabsch, 2010). The initial phase was determined by the molecular replacement method, using the Phaser program (McCoy et al., 2007). As the search models, the structure of the TacT dimer (Cheverton et al., 2016) (PDB ID: 5FVJ) [https://doi.org/10.2210/pdb5fvj/pdb] and the tRNA^{Gly}GCC model generated from the structure of tRNA^{Phe} (Byrne et al., 2010) (PDB ID: 3L0U) [https://doi.org/10.2210/pdb3l0u/pdb] were used. The structures were refined with Phenix.refine (Afonine et al., 2012), and manually modified with Coot (Emsley et al., 2010).

Crystallization and structure determination of AtaT2-AtaR2 complex

For the crystallization of the AtaR2-AtaT2 complex, 0.2 μL of 5 mg/ml AtaT2-AtaR2 protein solution was mixed with 0.2 μL of reservoir solution, containing 0.2 M potassium formate and 20% PEG 3350, and crystals were generated by the sitting drop vapor diffusion method at 20°C. Datasets were collected at beamline 17A at the Photon Factory at KEK, Japan. The crystals were flash-cooled in 1.1 × concentrated reservoir solution, supplemented with 20% (v/v) ethylene glycol as a cryoprotectant. The two datasets were collected from the crystals harvested from a single drop, and they were indexed, integrated, scaled with XDS, and merged using XSCALE. Since the diffraction data exhibited strong anisotropy, they were anisotropically corrected using the UCLA Diffraction Anisotropy Server (Strong et al., 2006). The homology models of AtaT2 and the RHH domain of AtaR2 were generated by the SWISS-MODEL server(Waterhouse et al., 2018), based on the structures of *S.* Typhimurium TacT (Cheverton et al., 2016) and a putative transcriptional factor from *Vibrio cholerae* (PDB ID: 1Y9B) [https://doi.org/10.2210/pdb1y9b/pdb], respectively, and were used as the search models. The structures were refined and manually modeled as described above.

In vitro transcription of tRNAs

tRNA^{Gly} variants, tRNA^{Arg}UCU, and tRNA^{Asn} were transcribed by T7 RNA polymerase. For tRNA^{Asn}, a precursor tRNA^{Asn} bearing the 5′-leader was synthesized and processed by RNaseP, comprising the M1 RNA and C5 protein (Yashiro et al., 2020). The synthesized tRNAs were purified on a Resource Q column (GE Healthcare, Japan) by a linear gradient of NaCl (0.2 - 1.0 M) in 20 mM Tris-HCl, pH 7.4. The DNA fragments encoding template sequences for *in vitro* transcription are listed in Table S2.

In vivo toxicity assay for TacT, AtaT2, and their variants

The toxicities of TacT, AtaT2, and their variants were examined as described (Yashiro et al., 2019, 2020; Zhang et al., 2020). *E. coli* strain MG1655 was transformed with pBAD33-TacT, pBAD33-AtaT2 or their variants, inoculated in LB containing 30 μg/ml chloramphenicol in the presence of 1% (w/v) glucose, and cultured at 37°C overnight. To test the toxicities of TacT or AtaT2 variants in the liquid medium, the overnight cultures were diluted to an OD_{660} of 0.02 in fresh liquid LB containing 30 μg/ml chloramphenicol and supplemented with 1% (w/v) glucose or 0.2 or 0.1% (w/v) arabinose. The cultures were continued at 37°C, and the OD_{660} values of the cultures were measured. To assess the toxicities of the TacT or AtaT2 variants by the spot assay, the overnight LB cultures were serially diluted, and 3 μL portions of the diluents were spotted on LB agar plates containing 30 μg/ml chloramphenicol and supplemented with 0.1% (w/v) arabinose, and then the plates were incubated at 37°C overnight.

QUANTIFICATION AND STATISTICAL ANALYSIS

We repeated the biochemical experiments in this study and the data represents the average of three independent experiments (n = 3) and the data presented with the SD of the independent experiments. Crystallographic structural statistics (Table1; Table S1) were analyzed using Phenix.